

<https://doi.org/10.1038/s43247-024-01354-2>

Triple oxygen isotope compositions reveal transitions in the moisture source of West China Autumn Precipitation

Check for updates

Lijuan Sha¹, Lijun Tian², Lifan Sha³, Yunxia Li⁴, Xuejie Wang⁵, Peng Hu^{6,7}, Qisheng Liang⁸, Baoyun Zong¹, Pengzhen Duan⁹ ✉ & Hai Cheng¹⁰ ✉

The isotopic composition has long been used to investigate the factors influencing precipitation, whereas the variations of event-based precipitation isotopes caused by moisture transition and synoptic meteorological conditions remain limited. Here we present triple oxygen and hydrogen isotopes in event-based precipitation during West China Autumn Precipitation to evaluate the influence of various moisture sources in the hydrological process. Isotopes $\delta^{18}\text{O}$, $\delta^{17}\text{O}$, and δD peak with convective precipitation at the onset stage, then drop to their lowest amid stratiform precipitation during the middle stage, and rise again towards the end. In contrast, $\Delta^{17}\text{O}$ levels remain elevated throughout the mid-stage of West China Autumn Precipitation compared to the onset and end stages. These isotopic variations, coupled with moisture analysis, reveal a distinct moisture source transition from the West Pacific Ocean to the westerly domain during West China Autumn Precipitation accompanied by the retreat of the Asian summer monsoon from Northwest China.

The Asian monsoon, an integral part of the global climate system, has been pivotal in facilitating climate change interactions between high- and low-latitude regions^{1,2}. The inland boundaries of the Asian summer monsoon are sensitive to monsoon and westerly variations, and the onset and retreat of the Asian summer monsoon are notably characterized by a prominent shift in moisture sources. Many studies have been conducted about the evolution of precipitation isotopes and their associations with moisture origins and local meteorological parameters^{3–7}, outlining the climatic patterns of transitional zones and dominant influencing factors. However, uncertainties regarding evaporating isotope ratios and the lack of isotope physics at small timescales still impede the comprehensive investigation into the estimated moisture sources⁸. To more specifically elaborate on the underlying mechanism and impact of the moisture source transition, it is necessary to employ a high-resolution precipitation sampling to illustrate the variations of stable isotopic composition in precipitation.

Stable isotopes of precipitation, such as oxygen ($\delta^{18}\text{O}$) and hydrogen (δD), are strongly influenced by the water vapor source and trajectory history, and thus can provide insight into precipitation's origin, transport, and transformation in the hydrological cycle^{9–13}. Combining the primary parameters $\delta^{18}\text{O}$ and δD , the deuterium excess ($d\text{-excess} = \delta\text{D} - 8 \times \delta^{18}\text{O}$)^{9,10} is typically regarded as a valuable parameter for investigating dynamic fractionation processes during evaporation^{14–17}, particularly given the influential role of relative humidity (RH) and air temperature on this proxy in moisture source regions^{14,18–20}. More recently, analytical advances have permitted obtaining precise measurements of the triple oxygen isotope composition ($\delta^{17}\text{O}$ and $\delta^{18}\text{O}$) of natural waters^{21–24}. The second-order isotopic parameter $\Delta^{17}\text{O}$, calculated as $[\Delta^{17}\text{O} = (\ln(\delta^{18}\text{O}/1000 + 1) - 0.528 \times \ln(\delta^{17}\text{O}/1000 + 1))]^{24,25}$, primarily reflects evaporation conditions with less temperature dependence than $d\text{-excess}$ ^{24–26}. Previous studies suggested that the $\Delta^{17}\text{O}$ in precipitation provides information on the evaporation conditions at the moisture source region (e.g., RH and turbulence), local

¹Institute of Global Environmental Change, Xi'an Jiaotong University, Xi'an, China. ²Center for Agricultural Resources Research, Institute of Genetics and Developmental Biology, Chinese Academy of Sciences, Shijiazhuang, China. ³Information Centre, Department of Natural Resources of Zhejiang Province, Hangzhou, China. ⁴College of Resources and Environmental Sciences, Hunan Normal University, Changsha, China. ⁵Institute of International Rivers and Eco-security, Yunnan University, Kunming, China. ⁶Yunnan Key Laboratory of Meteorological Disasters and Climate Resources in the Greater Mekong Subregion, Yunnan University, Kunming, China. ⁷Department of Atmospheric Sciences, Yunnan University, Kunming, China. ⁸Yunnan Key Laboratory of Plateau Geographical Processes & Environmental Changes, Faculty of Geography, Yunnan Normal University, Kunming, China. ⁹Research Institute of Petroleum Exploration and Development, PetroChina, Beijing, China. ¹⁰State Key Laboratory of Loess and Quaternary Geology, Institute of Earth Environment, Chinese Academy of Sciences, Xi'an, China. ✉e-mail: duanpengzhen@163.com; cheng021@xjtu.edu.cn

evaporation, moisture recycling, and mixing moisture sources at tropical and subtropical regions^{25,27–31}. However, only a few studies have considered the roles of cloud type (convective and stratiform precipitation)³² and cloud microphysics (such as sub-cloud re-evaporation)^{31,33} in determining the triple oxygen isotope composition of precipitation.

The West China Autumn Precipitation (WCAP) generally occurs at the end of the Asian summer monsoon^{34,35} and the synchronous commencement of the winter monsoon, with unique climatic characteristics resulting from diverse moisture sources and the trajectory of water vapor transport^{36,37}. Given the critical significance of WCAP in sustaining agricultural productivity and economic stability^{34,35,38}, it is vital to investigate its evolving patterns and moisture source transitions. Additionally, this research will provide a scientific basis for enhancing comprehension of intricate interactions between the westerly and monsoon systems. To better comprehend the factors influencing the WCAP, we present the temporal variations of $\delta^{18}\text{O}$, $\delta^{17}\text{O}$, δD , $\Delta^{17}\text{O}$, and d-excess evolution for event-based precipitation samples collected in Xi'an, located at the north margin of the WCAP area, from October 4th to 16th of 2021 and October 1st to 8th of 2022 to better understand the factors affecting the WCAP. Our high-resolution precipitation isotope data can provide valuable insights into the differential influences of stratiform and convective fractions on WCAP $\Delta^{17}\text{O}$ values. Furthermore, this dataset refined the interpretation of triple oxygen isotopes in precipitation, particularly in the context of moisture source transitions at the inland boundaries of the summer monsoon.

Materials and climatology

The sampling site (108.66°E, 34.26°N, 358 m a.s.l.) is located at the west of Xi'an city in Northwest China (Fig. 1). Located near the northwestern edge of the summer monsoon^{39,40}, the climatic patterns of the study site are predominantly controlled by the summer monsoon in summer and the westerly in non-monsoon seasons^{41,42}. Annual precipitation amount ranges from 500 to 700 mm, mostly occurring between July and October⁴³. Further precipitation may occur during November in some years following WCAP^{40,43}. The mean annual temperature is 13.5 °C, with winter being dry and cold, and summer characterized by hot and rainy conditions⁴⁰. In addition, a previous study⁴⁰ indicates that the temporal variation of $\delta^{18}\text{O}$ values in Xi'an precipitation displays an evident annual pattern: the highest values were observed between April and June, decreased throughout the monsoon season to reach their lowest values between July and October, and then increased again from November to April.

Results and discussion

The characteristics of meteorology

Figure 1 displays the daily meteorological characteristics (i.e., precipitation amount, temperature, RH, and air pressure) at the sample collection site during two WCAP periods: October 4th to 16th, 2021 and October 1st to 8th, 2022. In 2022, the precipitation amount increased from 6.3 mm on the 1st day to 23.3 mm on the 4th day, followed by a decrease to 3.1 mm on the 8th day, with the minimum being 2.1 mm on the 6th day. Concurrently, temperatures declined from 19.7 °C on the 1st day to 7.1 °C on the 5th day, and

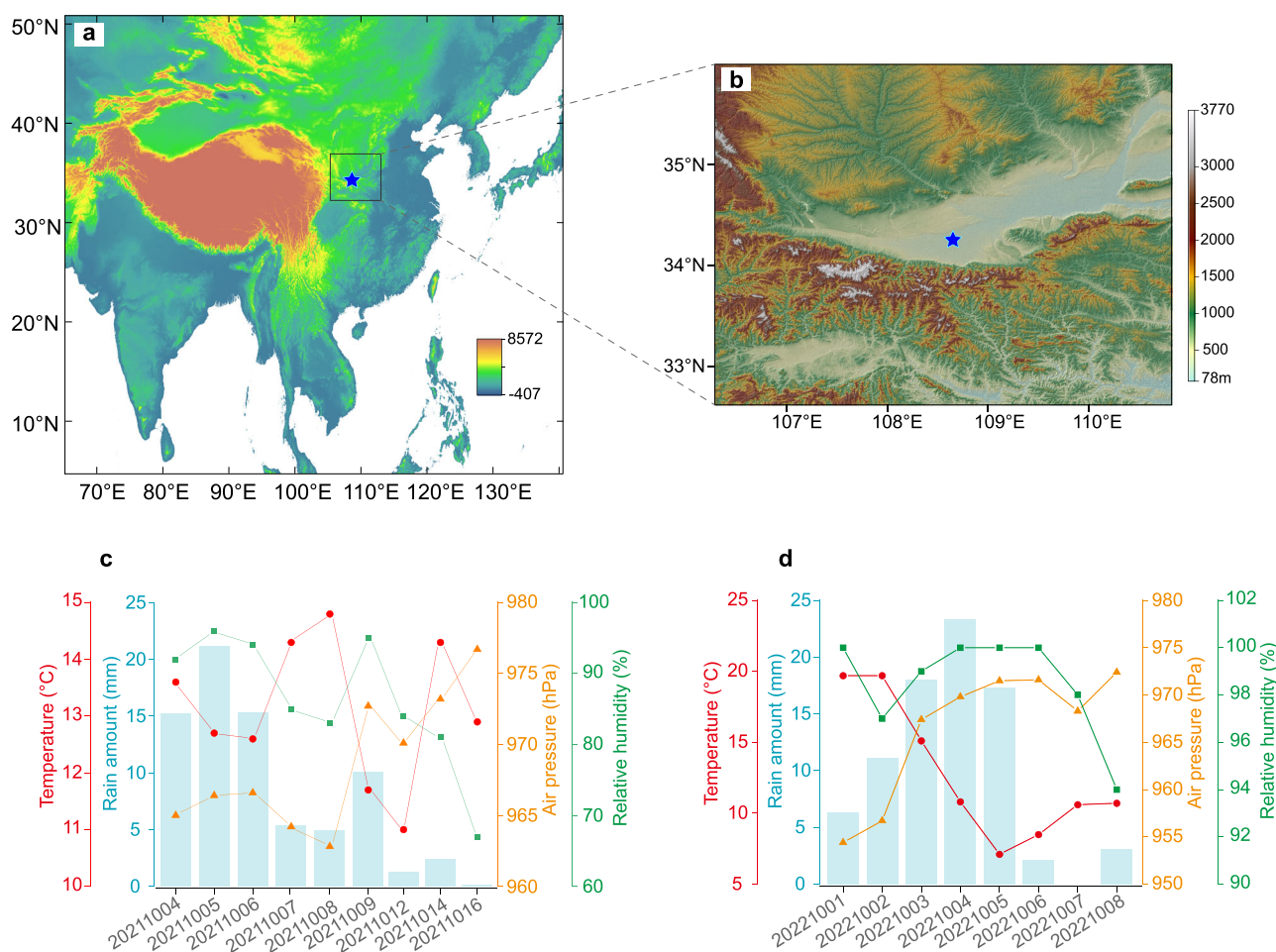


Fig. 1 | Geographic context and modern hydroclimate of the study area. Location (the blue star at 34.26°N, 108.66°E) (a) and topography of the study area (b). The topographic maps are from the Geospatial Data Cloud (<https://www.gscloud.cn/sources/>). The variations of temperature (red circles), relative humidity (green

squares), air pressure (orange triangles), and precipitation amount (cyan columns) in Xi'an during two West China Autumn Precipitation periods: October 4th to 16th, 2021 (c) and October 1st to 8th, 2022 (d).

then gradually ascended to 10.7 °C on the 8th day. The RH fluctuated between 94% and 100%, with an average of 98% during the WCAP in 2022 (Fig. 1d). The highest RH was documented on the 1st day, and the lowest temperature was on the 8th day. In contrast, the meteorological characteristics in 2021 manifested a more complex pattern (Fig. 1c). The higher precipitation amount was recorded on the 4th and 9th days, while high temperatures were observed on the 8th and 14th days. The RH varied from 67% (on the 4th day) to 96% (on the 16th day).

Asian summer monsoon weakens in intensity during late summer and early autumn, which prompts the formation of a low-pressure system over West China³⁶. The air pressure increased from 965 hPa on October 4th to 976 hPa on October 16th in 2021 (Fig. 1c). Similarly, the air pressure escalated from 954.4 hPa on October 1st to 971.6 hPa on October 6th in 2022 (Fig. 1d). The low-pressure system, particularly evident on October 4th and 5th, 2021 and October 1st and 2nd, 2022, attracted moist air from the West Pacific Ocean (Supplementary Figs. 1, 2), resulting in an increase in precipitation. Consistent with previous studies, it has been indicated that under the influence of easterly and southerly airflows from anomalous anticyclonic circulation, moisture from the West Pacific Ocean is transported toward West China^{34,37}. This influx increases local humidity and supplies an abundance of water vapor, thereby amplifying precipitation in the research region^{34,37}.

Moisture source analysis during WCAP

The reanalysis results of moisture uptake, based on the Hybrid Single-Particle Lagrangian Integrated Trajectory (HYSPPLIT) air mass back-trajectories (see details in Methods)⁴⁴, indicate diverse moisture sources during the WCAP period of both 2021 and 2022 years (Fig. 2). Vapor trajectories, traced back up to 120 h at 1500 m above ground level (a.g.l.), were delineated for the WCAP to account for the typical pattern of water vapor transport within the middle and lower troposphere⁴⁵. While the values representing the contribution of water vapor at 1500 m a.g.l. (Supplementary Fig. 3a) differ from the vapor trajectory calculations at 800 m a.g.l. (Supplementary Fig. 3b), both sets of air mass back-trajectory results reveal variations in moisture sources for the study area during the WCAP period.

During the pre-WCAP (October 4th, 2021 and October 1st to 3rd, 2022), the moisture sourced from the West Pacific Ocean primarily contributes to precipitation (Fig. 2). For instance, during the pre-WCAP stage of the year 2022 (October 1st to 3rd, 2022), the vapor trajectories calculation at 1500 m a.g.l. is estimated that approximately 42.3–97.7% of the water vapor contributing to precipitation is derived from the West Pacific Ocean (<33°N), while about 2.3–57.7% is sourced from Chinese inland water vapor (33°N–40°N) (Supplementary Fig. 3a). In addition, the moisture flux distribution map reveals that a substantial quantity of water vapor from the tropical regions of the West Pacific Ocean was transported to West China during the pre-WCAP (Supplementary Figs. 1, 2), carried by the easterly flow along the southern boundary of the Western Pacific Subtropical High (WPSH; Supplementary Figs. 4, 5). Notably, the position, shape, and intensity of the WPSH primarily govern the interannual variability of the large-scale, quasi-stationary East Asian summer monsoon frontal zones^{34,36}. The west and north sides of the WPSH are dominated by warm and humid air from oceans (Supplementary Figs. 4, 5), resulting in regions with higher precipitation⁴⁷. In addition to its seasonal latitudinal shifts, the WPSH exhibits short to medium-term fluctuations on timescales of one to two weeks⁴⁸. Furthermore, during the WCAP, cold and warm air activities are frequent in West China and meet to form frontal rain, which is conducive to the uplift of warm and humid airflow and easily forms precipitation⁴⁹.

During the mid-WCAP stage of the year 2022 (October 4th to 6th, 2022), the reanalysis results of moisture uptake indicate that water vapor from high-latitude sources (> 40°N) constitutes between 4.8% and 83.4% of the total. Subsequently, during the post-WCAP period of the year 2022 (October 8th, 2022), the inland water vapor contributes to 99% of the water vapor content (Supplementary Fig. 3a). This pronounced variability underscores a shift in moisture sources from high-latitude

regions to inland areas from mid-WCAP to post-WCAP. Such transition highlights the dynamics of moisture sourcing and its substantial impact on the regional water vapor composition during the WCAP. In addition, daily-scale analysis of the WPSH pattern indicates that the WPSH weakens and shifts southward during the mid- and post-WCAP period (spanning from October 7th to 16th of 2021 and 4th to 8th of 2022; Supplementary Figs. 4, 5; see details in “Methods”), concurrently causing southward shifts of the center of the westerly jet stream and facilitating the transport of water vapor from higher latitudes (Fig. 2). These circulation patterns illustrate that the interaction between warm and moist air from tropical oceans and cold water vapor sourcing from westerly/local regions contributes to precipitation.

Variations of precipitation isotopes

All the $\delta^{18}\text{O}$, $\delta^{17}\text{O}$, and δD manifested temporally coherent patterns (Fig. 3). In 2021, the WCAP isotope values fluctuated between -12.63‰ and -4.16‰ for $\delta^{18}\text{O}$, -6.66‰ and -2.20‰ for $\delta^{17}\text{O}$, -85.51‰ and -24.60‰ for δD . In 2022, the WCAP isotope values of $\delta^{18}\text{O}$, $\delta^{17}\text{O}$, and δD in precipitation varied between -18.89‰ and -7.44‰ and from -9.98‰ to -3.91‰ , -132.90‰ to -48.29‰ , respectively (Fig. 3). Higher $\delta^{18}\text{O}$ and δD values occur at the onset of rainfall, decline to the lowest in the mid-phase, and then exhibit an upward trend towards the end (Fig. 3).

The d-excess varied between 0.5‰ and 21.2‰ in 2021 and from 6.5‰ to 18.2‰ in 2022 (Fig. 3), with mean values of $14.6 \pm 5.9\text{‰}$ and $14.1 \pm 3.7\text{‰}$ for the respective years, which was slightly higher than the global average of 10‰⁹. In addition, $\Delta^{17}\text{O}$ varies from -1 to 44 per meg in 2021 and from 15 to 52 per meg in 2022 (Fig. 3). The average $\Delta^{17}\text{O}$ values are 26 ± 11 per meg and 36 ± 10 per meg for the years 2021 and 2022, respectively. Notably, these values align with the $\Delta^{17}\text{O}$ values of modern meteoric waters in non-polar regions, which typically range between 20–30 per meg according to recent compilations and long-term records^{30,31,50–52}.

Relationship between isotope composition and meteorological data

To gain a deeper understanding of the variables influencing the WCAP isotope values, we investigated their relationships with temperature, RH, precipitation amount, and air pressure at the sampling site (Fig. 4). In 2022, $\delta^{18}\text{O}$ exhibits a positive correlation with temperature ($r = 0.956$), consistent with the established understanding that higher temperatures typically lead to enriched $\delta^{18}\text{O}$ values due to increased evaporation and fractionation effects. However, the absence of a negative correlation between d-excess and temperature, and between $\Delta^{17}\text{O}$ and d-excess, suggests that the isotopic signatures we observed are more likely influenced by rainout processes and the temperature-dependent fractionation of isotopes during precipitation formation, rather than evaporation effects alone. Moreover, the Rayleigh distillation effect, where higher temperatures reduce rainout during air mass transport, leads to enriched $\delta^{18}\text{O}$ values in precipitation. Conversely, in 2021, the correlation is not significant ($r = 0.121$) (Fig. 4). This divergence may be attributed to the unique regional temperature patterns during that year, suggesting that temperature may not be the primary controlling factor in the isotopic variation in precipitation in the sub-tropical region. Furthermore, there is a notable negative correlation between $\delta^{18}\text{O}$ and RH ($r = -0.607$) in 2021, whereas in 2022, this correlation is not significant ($r = -0.307$) (Fig. 4). While lower RH is generally associated with enriched $\delta^{18}\text{O}$ values due to enhanced evaporation and fractionation, the observed correlations indicate that the relationship can be complex and is not consistently observed across different years. In contrast, there was no clear correlation between these isotope values and precipitation amounts during the two WCAP periods (Fig. 4). Indeed, variations in the source area of water vapor and large-scale convection processes are closely linked to the stable isotope characteristics of precipitation in the Asian monsoon region⁵³. Factors such as water vapor transport distance and Rayleigh distillation during the water vapor transport also influence the levels and characteristics of stable isotopes in modern precipitation^{54,55}. Generally, $\delta^{18}\text{O}$, $\delta^{17}\text{O}$, and δD values in precipitation decrease with increased water vapor transport

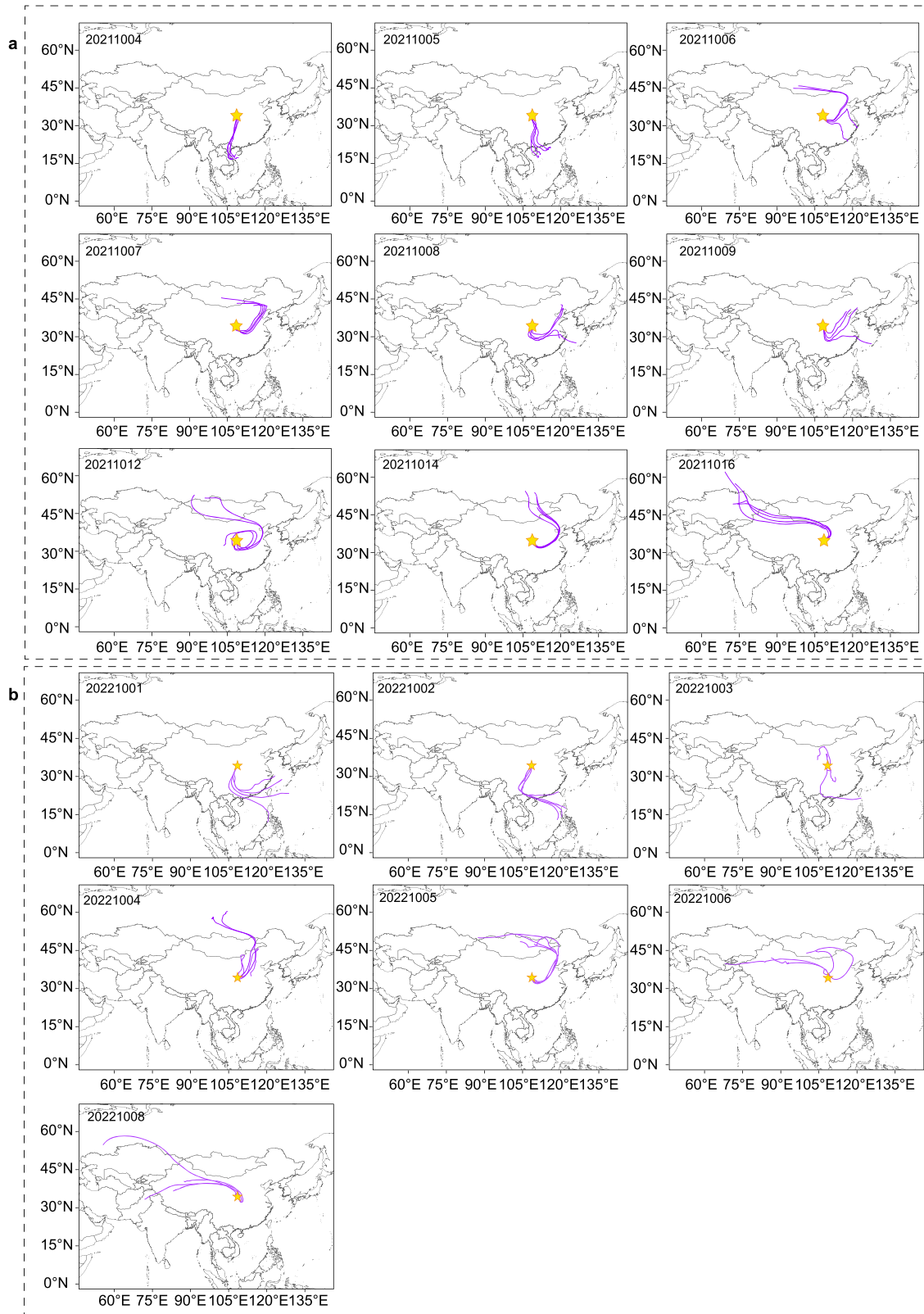


Fig. 2 | Back-trajectories starting at Xi'an for each West China Autumn Precipitation event in 2021 and 2022. The reanalyses were based on the HYSPLIT model during the West China Autumn Precipitation from October 4th to 16th, 2021 (a) and October 1st to 8th, 2022 (b), respectively. Back-trajectories (120-hour) were computed using the HYSPLIT model⁴⁴ based on National Center for Environmental

Prediction/National Center for Atmospheric Research (NCEP/NCAR) reanalysis data (https://ready.arl.noaa.gov/HYSPxT_traj.php). The contribution of water vapor at 1500 m above ground level (a.g.l.) offers a macroscopic view of vapor movement patterns. The yellow star indicates the sampling site (34.26°N, 108.66°E).

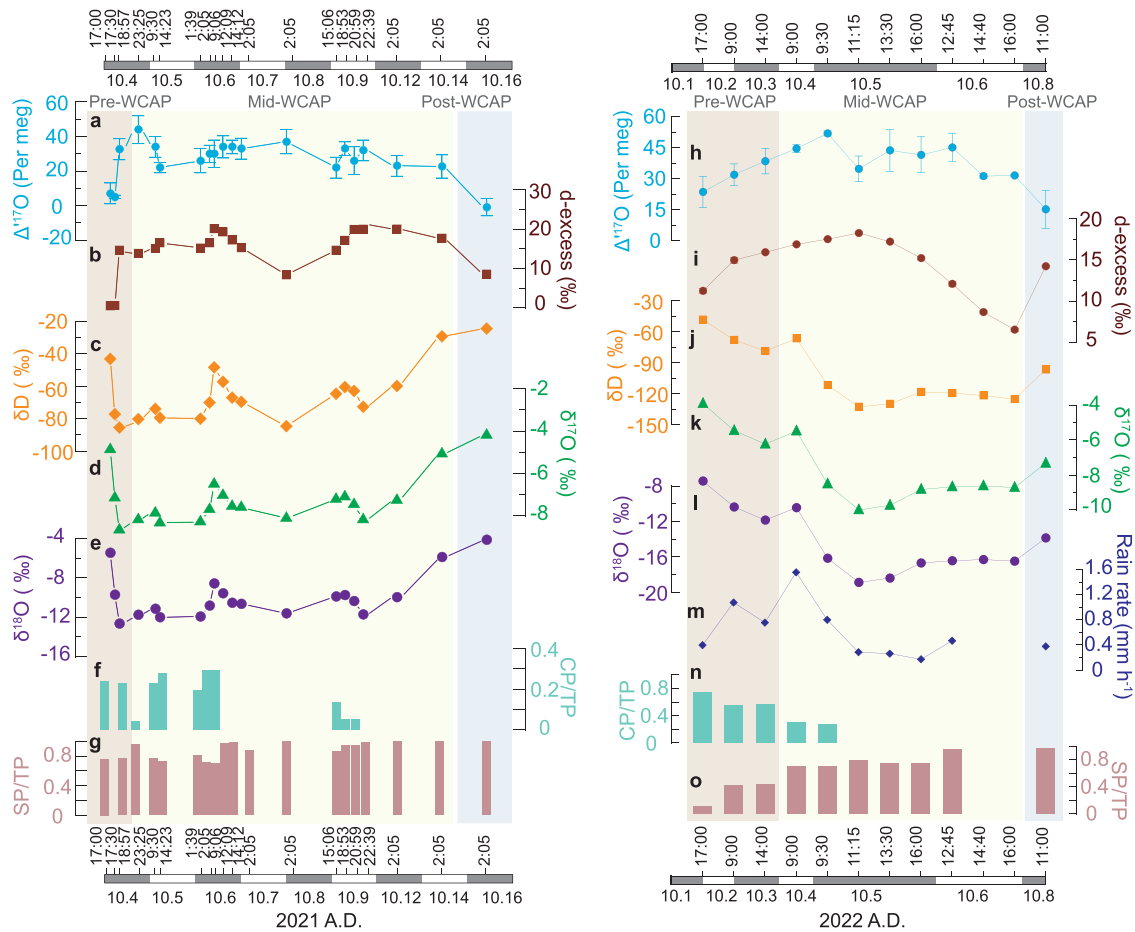


Fig. 3 | Temporal variations of meteorological factors and triple oxygen and hydrogen isotopes of precipitation. **a** and **h** $\Delta^{17}\text{O}$, **b** and **i** d-excess, **c** and **j** δD , **d** and **k** $\delta^{18}\text{O}$, **e** and **l** $\delta^{18}\text{O}$, **m** rain rate in the study area during two West China Autumn Precipitation (WCAP) periods: October 4th to 16th, 2021 and October 1st to 8th, 2022. The parameters of convective precipitation (CP), stratiform precipitation (SP; also known as large-scale precipitation) and total precipitation (TP) denote the

accumulated precipitation that descends to the Earth’s surface and are derived from the cloud scheme within the ECMWF Integrated Forecasting System (IFS). **f** and **n** The ratio of convective precipitation and total precipitation (CP/TP), **g** and **o** The ratio of stratiform precipitation and total precipitation in the study area during the WCAP. The shades indicate pre-WCAP (pink), mid-WCAP (yellow), and post-WCAP (light blue), respectively.

distance. Additionally, depleted isotopic signatures also occur during prolonged rain events spanning several days⁵⁶.

In terms of second-order parameters, we observe a positive correlation between $\Delta^{17}\text{O}$ values in precipitation and RH for the 2021 and 2022 samples. However, when examining correlations with other local meteorological factors (temperature, precipitation amount, and air pressure; Fig. 4), both d-excess and $\Delta^{17}\text{O}$ values of precipitation show weak correlations. This observation may imply that local processes besides RH exert minimal influence on these specific second-order parameters.

Controls on precipitation isotopes

During the WCAP for both 2021 and 2022, co-variations were observed in $\delta^{18}\text{O}$, $\Delta^{17}\text{O}$, and d-excess, with a negative correlation between $\delta^{18}\text{O}$ and both $\Delta^{17}\text{O}$ ($r = -0.698$ and -0.343 for 2021 and 2022, respectively) and d-excess ($r = -0.355$ and -0.068 for 2021 and 2022, respectively; Fig. 4), as well as a positive correlation between $\Delta^{17}\text{O}$ and d-excess ($r = 0.61$ and 0.43 for 2021 and 2022, respectively; Fig. 4 and Supplementary Fig. 6). Furthermore, the slope relating d-excess and $\Delta^{17}\text{O}$ across all WCAP precipitation samples for both 2021 and 2022 was consistent at 1.2 per meg/‰ (Supplementary Fig. 6). This pattern suggests the possibility of both surface and sub-cloud re-evaporation processes during the WCAP^{57,58}; however, these were not the only mechanisms influencing the variations in $\Delta^{17}\text{O}$ values observed in this study⁵⁸. Other contributing factors, such as atmospheric conditions at the moisture source, large-scale processes along the moisture transport

trajectories, and upstream convection, can also play roles in controlling the isotopic composition of precipitation at different stages of the WCAP. Therefore, the factors influencing the evolution of precipitation isotopes at various stages of WCAP can be summarized as follows:

At the onset of the pre-WCAP stage (October 4th, 2021 and October 1st to 3rd, 2022), the precipitation isotopes exhibited higher $\delta^{18}\text{O}$ and δD values, and as the stage progressed, there was a noticeable reduction in these values (Fig. 3). During this stage, the sub-cloud re-evaporation during precipitation affects the raindrops from small rainfall events, leading to strong isotopic dynamic fractionation^{33,58}, characterized by an inverse correlation between $\Delta^{17}\text{O}$ and $\delta^{18}\text{O}$ but a positive correlation between $\Delta^{17}\text{O}$ and d-excess in precipitation. During sub-cloud re-evaporation, kinetic fractionation results in the evaporated vapor exhibiting a positive $\Delta^{17}\text{O}$, and this process, in turn, leads to a decrease in $\Delta^{17}\text{O}$ in the residual raindrop^{25,28,51,59}. Moreover, the reanalysis results from HYSPLIT reveal that moisture, intermittently sourced from the West Pacific Ocean, primarily contributes to precipitation during the pre-WCAP stage. During this stage, the high air temperature and low air pressure at the study site (Fig. 1) could promote the ascent and condensation of warm and moist air from the West Pacific Ocean, leading to convective precipitation. These convective conditions result in the lifting of lower-layer water vapor with enriched isotopes through updrafts, resulting in the relatively high $\delta^{18}\text{O}$ values in precipitation^{60,61} and correspondingly relative low $\Delta^{17}\text{O}$ and d-excess values³¹ (Fig. 3).

Following the pre-WCAP stage, the $\delta^{18}\text{O}$ and δD values decrease by 8‰ and 90‰, and $\Delta^{17}\text{O}$ values increase ~15 per meg, respectively (Fig. 3).

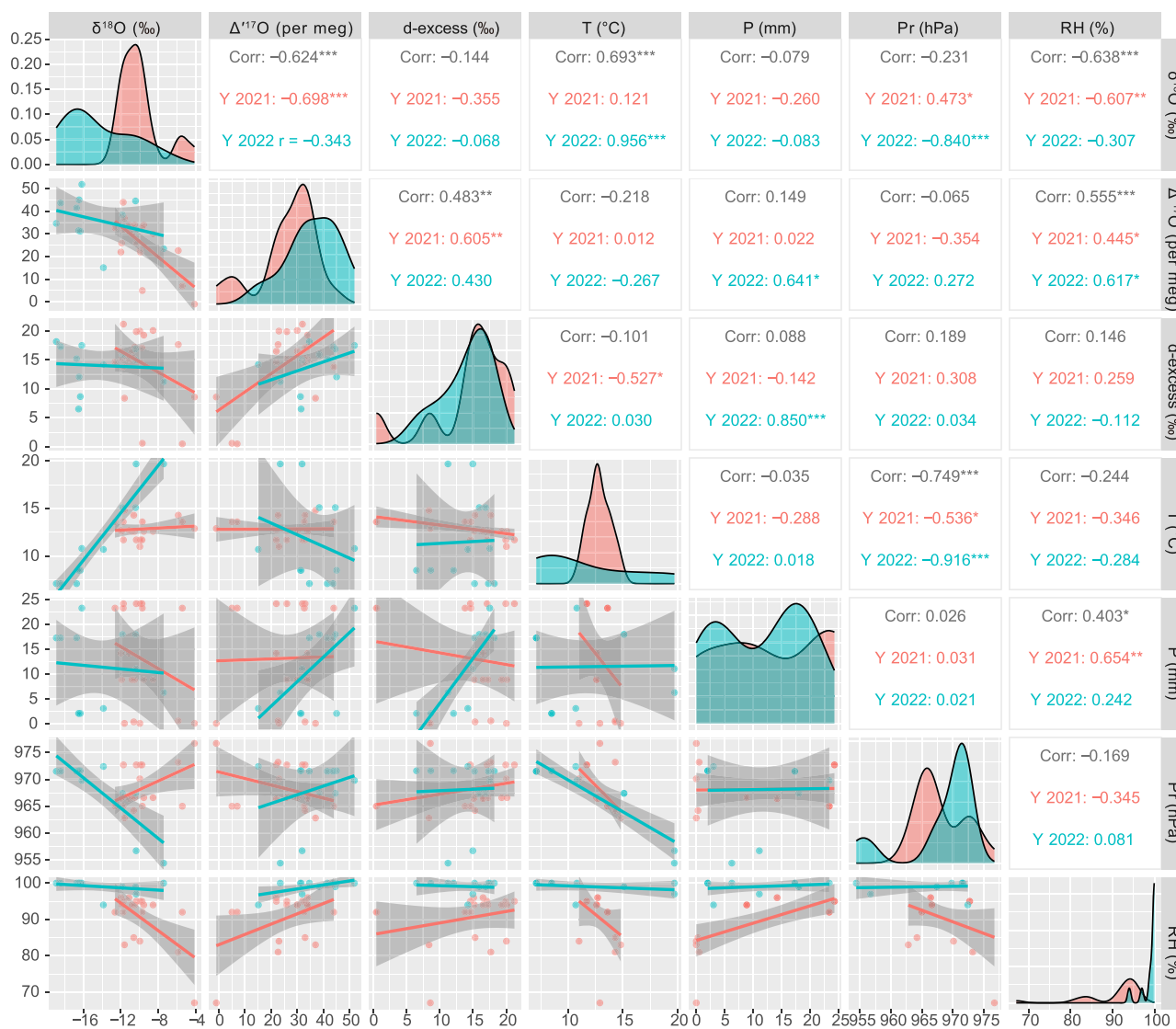


Fig. 4 | Correlations of $\delta^{18}\text{O}$, $\Delta^{17}\text{O}$ and d-excess vs temperature, precipitation amount, air pressure and relative humidity in 2021 and 2022. Red and blue colors represent correlation values for 2021 and 2022, respectively, while gray indicates the

correlation values for both years. $\Delta^{17}\text{O} = (\delta^{17}\text{O} - 0.528 \times \delta^{18}\text{O}) \times 1000$, where $\delta^{17}\text{O} = 1000 \times \ln(1 + \delta^{17}\text{O}/1000)$ and $\delta^{18}\text{O} = 1000 \times \ln(1 + \delta^{18}\text{O}/1000)$.

During the pre-WCAP period, continuous rainfall occurs over several days, causing saturation or near-saturation of water vapor at the base of the atmosphere to approach or attain saturation, thereby reducing evaporation to near zero (Fig. 1), and thus the raindrops gradually evolve to achieve the isotopic equilibrium with ambient water vapor without re-evaporation, a process referred to as equilibration^{62,63}. The isotopic evolution of falling raindrops is also affected by the isotopic composition of sub-cloud water vapor, which is highly variable within and among precipitation events^{54,55,64}. The decrease in $\delta^{18}\text{O}$ and a concomitant slight increase in $\Delta^{17}\text{O}$ may correlate with an increased total precipitation amount for this specific rain event. This correlation draws upon the principles of Rayleigh distillation as a fundamental mechanism behind the precipitation amount effect^{54,55}. We align these observations with the Rayleigh distillation model, as precipitation intensifies, the fraction of remaining vapor (f) in Rayleigh distillation diminishes, thus affecting the isotopic composition of raindrops³³, in which increased precipitation amount leads to a decrease in $\delta^{18}\text{O}$ and a correlated slight increase of $\Delta^{17}\text{O}$. The large decrease in $\delta^{18}\text{O}$ observed in our study primarily reflects the influence of condensation processes. This is because $\delta^{18}\text{O}$, along with $\delta^{17}\text{O}$ and δD , which are primary isotope parameters, are altered during condensation process. As moisture undergoes rainout, Rayleigh distillation leads to precipitation being enriched in heavy isotopes,

while the remaining water vapor becomes increasingly depleted in these isotopes. Consequently, precipitation formed at subsequent stages of the rainout process exhibits lower $\delta^{18}\text{O}$ values compared to earlier precipitation, illustrating the progressive depletion of heavy isotopes in the remaining water vapor. Conversely, evaporation processes have a more pronounced effect on secondary isotope parameters, such as d-excess and $\Delta^{17}\text{O}$. These parameters are sensitive to the kinetic effects that occur during evaporation, especially under conditions of low humidity and non-equilibrium states. The d-excess and $\Delta^{17}\text{O}$ values increase in response to reduced evaporation, indicative of higher relative humidity conditions at the evaporation site^{31,33}. Moreover, terrestrial moisture recycling (including evapotranspiration, evaporation, and sublimation of snowfields) could also contribute to the higher $\Delta^{17}\text{O}$ values to some extent^{29,31,65}.

During the mid- and post-WCAP stages (spanning from October 7th to 16th of 2021 and 4th to 8th of 2022), relatively low $\delta^{18}\text{O}$ (−20‰ to −10‰) and δD (−120‰ to −60‰) values and high $\Delta^{17}\text{O}$ values are found in the precipitation. In these stages, stratiform precipitation is the predominant form (Fig. 3). Studies indicate a decrease in precipitation $\delta^{18}\text{O}$ ^{60,61} and an increase in $\Delta^{17}\text{O}$ ^{31,32} as the proportion of stratiform precipitation, primarily sourced from tropospheric moisture^{32,60,66}. Additionally, previous research in the Western Himalayas highlighted isotopically depleted weighted

average $\delta^{18}\text{O}$ values in precipitation during westerly periods (-17.1‰ to -10.2‰), contrasting with those during southwest monsoon periods, which range from -11.2‰ to -5.2‰ ⁶⁷. Thus, the vertical motion of the air in the stratiform clouds enables water vapor with relatively depleted isotopes to converge in the upper atmospheric layer^{60,61}, and different moisture sources could affect the precipitation isotope compositions.

During the mid-WCAP period, the observed mean $\Delta^{17}\text{O}$ values in precipitation were 30 and 40 per meg for the years 2021 and 2022 respectively, exceeding the estimated $\Delta^{17}\text{O}$ value of 15 per meg from precipitation formed through water vapor evaporation from the West Pacific Ocean under the RH of 72% (Supplementary Figs. 8, 9). Further, the reanalysis results of air mass back-trajectories (Fig. 2) indicate that high-latitude air masses and continental sources play a critical role during the mid- and post-WCAP stages of both 2021 and 2022. These findings suggest that the primary moisture source is not the West Pacific Ocean. Instead, the high precipitation $\Delta^{17}\text{O}$ values observed during the mid-WCAP stage can be attributed to westerly water vapor resulting from extended moisture trajectories and continental moisture recycling. As supporting evidence, the high-latitude surface snow and water vapor at Northwest Greenland (North Greenland Eemian Drilling Project; NEEM) have higher $\Delta^{17}\text{O}$ values during autumn and winter, with an average value of ~ 40 per meg⁶⁸. Further corroboration derives from triple oxygen isotope records from the USA²⁹, where precipitation in high-latitude areas that are usually dominated by the westerly displays elevated $\Delta^{17}\text{O}$ values (31–43 per meg), indicating the contribution of high-latitude continental recycled moisture carried by the westerly.

In our study region, the linear regression equation between $\delta^{18}\text{O}$ and δD during the stratiform precipitation period in 2022 and 2021 is presented by: $\delta\text{D} = 8.13 \times \delta^{18}\text{O} + 16.25$ ($n = 11$, $r = 0.99$) and $\delta\text{D} = 7.66 \times \delta^{18}\text{O} + 12.01$ ($n = 18$, $r = 0.96$), respectively (Supplementary Fig. 6). The slopes and the intercepts of both years are higher than the local meteoric water line $\delta\text{D} = 7.5 \times \delta^{18}\text{O} + 7.4$ ($n = 168$, $r = 0.97$) in precipitation data of monsoon season from 2016 to 2020 in Xi'an⁴⁰, indicating that the moisture recycling or moisture source change may cause the variations of our event-based samples. Deviations of the Local Meteoric Water Line in the Mid-WCAP from the Global Meteoric Water Line ($\delta\text{D} = 8 \times \delta^{18}\text{O} + 10$)⁹ are contingent upon factors such as condensation temperature, moisture source, transport path, and changes in climatic conditions⁶⁹. The higher intercepts of the regression equation of both years (Supplementary Fig. 6) suggested the contribution of precipitation from the westerly moisture source disturbances⁶⁷. Moreover, the transition from mid-WCAP to post-WCAP is characterized by a change in moisture sources, moving from high-latitude regions to inland areas (Supplementary Fig. 3). This highlights the importance of moisture recycling, where water vapor evaporates and precipitates within the same air mass across continents, potentially resulting in distinct isotopic compositions and higher intercepts in our regression equations.

On the other hand, the relationship between $\delta^{17}\text{O}$ and $\delta^{18}\text{O}$ values in precipitation ($\delta^{17}\text{O} = 0.527 \times \delta^{18}\text{O} + 0.22$ for 2021 and $\delta^{17}\text{O} = 0.528 \times \delta^{18}\text{O} + 0.03$ for 2022; Supplementary Fig. 6) is close to the Global Meteoric Water Line ($\delta^{17}\text{O} = 0.528 \times \delta^{18}\text{O} + 0.033$)²⁵. Accordingly, this alignment suggests that the processes affecting the isotopic composition of precipitation in our study are representative of global meteorological processes. The study underscores the dominance of large-scale processes on the isotopic composition of the original water vapor (Supplementary Fig. 7), including different moisture trajectories, evaporative conditions at the moisture source, and recycling along trajectories^{51,70}. Notably, slight deviations in the intercepts for both years could be indicative of minor variations in local climatic conditions, such as changes in relative humidity, temperature, or precipitation amount at the study site or alterations in the recycling pathways.

Conclusions

This study analyzed the stable isotopes ($\delta^{18}\text{O}$, $\delta^{17}\text{O}$, and δD) and associated second-order isotopic parameters ($\Delta^{17}\text{O}$ and d-excess) in event-based

precipitation samples collected at Xi'an in Northwest China during two WCAP periods on October 4th to 16th, 2021 and October 1st to 8th, 2022. For the WCAP rain events, the correlations between stable isotopic data and local meteorological parameters, such as precipitation amount, RH, and air pressure, are either weak or non-existent.

Our results showed that the temporal isotope variability during the WCAP was affected by the transitions of moisture sources between the West Pacific Ocean and regional and high-latitude atmospheric circulation patterns. During the pre-WCAP period, higher $\delta^{18}\text{O}$, $\delta^{17}\text{O}$, and δD values and lower $\Delta^{17}\text{O}$ and d-excess values result from sub-cloud evaporation and convective precipitation. During the mid-WCAP and post-WCAP periods, stratiform precipitation predominates, resulting in the lowest $\delta^{18}\text{O}$, $\delta^{17}\text{O}$, and δD values. The relatively high $\Delta^{17}\text{O}$ and d-excess values during the mid-WCAP correlate with moisture sources transported by westerly. Therefore, in combination with air mass back-trajectories, the triple oxygen isotope composition of precipitation can be a tracer of rainfall activity and the transition of moisture sources. The precipitation $\Delta^{17}\text{O}$ variations offer insights into the movement of air masses and provide a basis for future research, contextualizing moisture sources in relation to changes in precipitation patterns.

Methods

Precipitation sampling and analysis

The precipitation samples were collected by a bucket placed on the roof of the building from October 4th to 16th, 2021 and October 1st to 8th, 2022. The samples were collected after each precipitation event, and eight buckets were used to alternate between hourly collections. The collected precipitation was transferred to a 10 ml bottle for spare, and five aliquots of each sample were stored in 2 ml glass bottles for measurements. No headspace was allowed in glass vials to avoid evaporation. The glass vials were stored in a refrigerator at 4 °C for further isotopic analysis.

The $\delta^{18}\text{O}$, $\delta^{17}\text{O}$, and δD values were measured using Picarro-L2140i at the Xi'an Jiaotong University Isotope Laboratory, Xi'an, China. Each sample was measured three times. In order to avoid the memory effect associated with the continuous flow method, ten injections were conducted every time, and the first three measurements were discarded^{3,22}.

Notations in the triple oxygen isotope system

The isotope ratios ($\delta^{18}\text{O}$, $\delta^{17}\text{O}$, and δD) are reported using the δ notation defined by the following equation:

$$\delta = (R_{\text{sample}}/R_{\text{standard}} - 1) \times 1000 \quad (1)$$

where R_{sample} and R_{standard} represent the ratios ($^{18}\text{O}/^{16}\text{O}$, $^{17}\text{O}/^{16}\text{O}$ or $^2\text{H}/^1\text{H}$) of the samples and the Vienna Standard Mean Ocean Water (VSMOW) standard, respectively. The δ notation is expressed as per mil (parts per thousand, ‰).

The d-excess is expressed as the following equation⁹:

$$d - \text{excess} = \delta\text{D} - 8 \times \delta^{18}\text{O} \quad (2)$$

The definition of $\Delta^{17}\text{O}$ defines the deviation of triple oxygen isotope data from a reference relationship between $\delta^{17}\text{O}$ and $\delta^{18}\text{O}$, which is expressed in the linearized form⁷⁰:

$$\Delta^{17}\text{O} = (\delta^{17}\text{O} - 0.528 \times \delta^{18}\text{O}) \times 1000 \quad (3)$$

where $\delta^{17}\text{O} = 1000 \times \ln(1 + \delta^{17}\text{O}/1000)$ and $\delta^{18}\text{O} = 1000 \times \ln(1 + \delta^{18}\text{O}/1000)$. The value of 0.528 is the slope of the $\delta^{18}\text{O}$ - $\delta^{17}\text{O}$ reference line commonly used in hydrological studies²⁵. $\Delta^{17}\text{O}$ values are generally tiny and expressed in units of per meg (10^{-3} per mil).

The results were calibrated against the VSMOW and SLAP standards by a two-point calibration, with $\delta^{18}\text{O}$, $\delta^{17}\text{O}$ and δD values as follows: VSMOW (0‰, 0‰, 0‰) and SLAP (-55.5‰ , -29.69865‰ , -427.5‰)⁷¹. We also employed three working standards with $\delta^{18}\text{O}$, $\delta^{17}\text{O}$ and δD values as follows: LAB1 (-1.270‰ , -0.680‰ , -11.6‰), LAB2 (-11.651‰ ,

−6.141‰, −78.7‰) and LAB3 (−17.619‰, −9.315‰, −134.7‰). The analytical precisions (1σ SD) were better than ±0.025‰ for δ¹⁷O/δ¹⁸O and ±0.1‰ for δD²². Typical in-sample Δ¹⁷O and d-excess precisions (1σ SD) in water standards were 10 per meg and 0.1‰, respectively.

Calculation of Δ¹⁷O based on the relative humidity

The Δ¹⁷O in ocean surface water vapor [Δ¹⁷O(v)] can be assessed by relative humidity over ocean surface based on a closure assumption that vapor in the boundary layer is derived from evaporation only³⁰. Following previous studies^{24,25,30}, we use hn instead of ordinary relative humidity (h), where hn is the ratio of vapor concentration of free air to saturated concentration at the temperature and salinity of the ocean surface. The calculation of Δ¹⁷O (v) values is based on the following equation²⁶:

$$\Delta^{17}\text{O}(\text{v}) = -\ln((^{18}\alpha_{\text{eq}}^{0.529} (^{18}\alpha_{\text{diff}}^{0.518} (1-h_n) + h_n)) + 0.528 \times \ln(^{18}\alpha_{\text{eq}} (^{18}\alpha_{\text{diff}} (1-h_n) + h_n)))$$

where ¹⁸α_{eq} and ¹⁸α_{diff} are equilibrium and diffusion factors between ¹⁸O and ¹⁶O, respectively. Here, we calculated hn using a constant ¹⁸α_{eq} value of 1.0094³⁰ and ¹⁸α_{diff} value of 1.0096²⁵. The 5 per meg (Δ¹⁷O_(ocean/VSMOW)) was added to the estimated Δ¹⁷O data of precipitation to correct the difference between seawater and V-SMOW²⁵. Secondly, the vapor Δ¹⁷O(v) value was corrected for the closure assumption bias (Δ_{closure} = 3 per meg)³⁰.

In estimating Δ¹⁷O, we compiled data throughout the entire period of the mid-WCAP for 2021 and 2022, utilizing the measurement values of precipitation Δ¹⁷O. The uncertainties in our estimates for RH and temperature primarily originate from the limited spatial and temporal resolution of the meteorological data, the inherent variability in atmospheric conditions, and the uncertainties in the models. While these datasets do not explicitly quantify the uncertainty in RH and temperature, it is important to note that the precipitation Δ¹⁷O values predominantly reflect the evaporation conditions in the moisture source regions and exhibit less dependence on temperature variations.

The relative humidity values for the West Pacific Ocean were obtained from NOAA.

Meteorological data

Meteorological data at the station, such as precipitation amount, temperature, relative humidity, and air pressure, were obtained from the National Climate Center (<http://cmdp.ncc-cma.net>).

Analysis of convective precipitation and stratiform precipitation

The datasets of daily mean precipitation employed in this paper were from the National Centers for Environmental Prediction-Department of Energy (NCEP-DOE) reanalysis data⁷², which includes convective precipitation, stratiform precipitation (also known as large-scale precipitation), and total precipitation. The precipitation data is on a T62 (192 × 94) Gaussian grid.

Convective precipitation and stratiform precipitation: These parameters denote the accumulated precipitation that descends to the Earth's surface and are derived from the cloud scheme within the European Center for Medium-Range Weather Forecasts (ECMWF) Integrated Forecasting System. Specifically, convective precipitation arises from the convection scheme, while stratiform precipitation is a product of the cloud scheme. The cloud scheme in the Integrated Forecasting System encapsulates the genesis and dissipation of clouds. Both convective precipitation and stratiform precipitation are influenced by variations in atmospheric metrics such as pressure, temperature, and moisture, which are directly forecasted at the spatial dimensions of the grid box or larger scales. The other method for calculating convective precipitation, stratiform precipitation, and total precipitation data is extracted from ERA5 (<https://cds.climate.copernicus.eu/>)⁷³, the latest (fifth) generation of reanalysis data product provided by the European Center for Medium-Range Weather Forecasts. The spatial and temporal resolution of ERA5

reanalysis data product is 0.25° × 0.25° and hourly, respectively. The time used in this study refers to the local solar time (UTC + 8). Besides, ERA5 is highly sensitive and reliable for precipitation reproduction⁷⁴. Here, we selected the whole region of Xi'an city (33°N–35°N, 107°E–110°E) as the extracting object, and GRADS and MATLAB softwares were used to read and write these original data from ERA5.

Analysis of the western pacific subtropical high

To investigate the variation of vapor sources of precipitation in the sampling site, we graph the pattern of the Western Pacific Subtropical High (WPSH) daily. The 5880 geopotential meter (gpm.) was applied to define the periphery of the WPSH, and the geopotential high and the vector wind date at 500 hPa level are from National Center for Environmental Prediction Research, NCEP reanalysis data (<https://psl.noaa.gov/data/gridded/data.ncep.reanalysis2.html>)⁷⁵.

Moisture sources analysis

The reanalysis of the moisture uptake was assessed by the HYSPLIT model⁴⁴ (Fig. 2). The trajectory calculation of moisture source regions was performed at a one-hour time interval during precipitating days, and the back trajectory of the air mass (at 1500 m a.g.l.) was calculated until 120 h before the precipitation event occurred. The moisture calculated at 1500 m a.g.l. in this study, offers a macroscopic view of vapor movement patterns⁴⁵. We followed the method developed by previous methods^{76,77} to identify the moisture uptake locations along the moisture trajectories. Briefly, a more conservative threshold of the positive gradient in specific humidity (0.2 g kg⁻¹ in 6 h) and an initial relative humidity higher than 80% were employed as two criteria to identify moisture uptake locations⁷⁶. Grids of 2 × 2° were used to compute the moisture uptake locations, and the shading degree indicates the relative contribution of each grid to the precipitation event.

Reporting summary

Further information on research design is available in the Nature Portfolio Reporting Summary linked to this article.

Data availability

All precipitation isotopic data presented in this paper are available online on the Figshare database (<https://doi.org/10.6084/m9.figshare.25374475>). The moisture back-trajectories were computed using the NOAA HYSPLIT model based on Environmental Prediction/National Center for Atmospheric Research, National Centers for Environmental Prediction/National Center for Atmospheric Research (NCEP/NCAR) reanalysis data (https://ready.arl.noaa.gov/HYSPxT_traj.php). Reanalyzed relative humidity, moisture flux and the Western Pacific Subtropical High based on the data from the National Centers for Environmental Prediction/National Center for Atmospheric Research, NCEP/NCAR (<https://www.esrl.noaa.gov>). The dataset for convective precipitation, stratiform precipitation, and total precipitation is extracted from ERA5 (<https://cds.climate.copernicus.eu/>). The geographic map was obtained from NOAA National Centers for Environmental Information (<https://www.ncei.noaa.gov/products/etopo-global-relief-model>).

Received: 12 July 2023; Accepted: 28 March 2024;

Published online: 09 April 2024

References

- Cheng, H. et al. The Asian monsoon over the past 640,000 years and ice age terminations. *Nature* **534**, 640–646 (2016).
- Wang, P. X. Global monsoon in a geological perspective. *Chin. Sci. Bull.* **54**, 1113–1136 (2009).
- Sha, L. J. et al. Variations in triple oxygen isotope of speleothems from the Asian monsoon region reveal moisture sources over the past 300 years. *Commun. Earth Environ.* **4**, 384 (2023).
- Ding, Y. The variability of the Asian Summer Monsoon. *J. Meteor. Soc. Jpn.* **85B**, 21–54 (2007).

5. Dong, G. et al. CMIP5 model-simulated onset, duration and intensity of the Asian summer monsoon in current and future climate. *Clim. Dyn.* **46**, 355–382 (2016).
6. Li, J. & Zhang, L. Wind onset and withdrawal of Asian summer monsoon and their simulated performance in AMIP models. *Clim. Dyn.* **32**, 935–968 (2009).
7. Chen, L., Chen, W., Hu, P., Chen, S. & An, X. Climatological characteristics of the East Asian summer monsoon retreat based on observational analysis. *Clim. Dyn.* **60**, 3023–3037 (2023).
8. Ichiyanagi, K., Yoshimura, K. & Yamanaka, M. D. Validation of changing water Origins over Indochina during the withdrawal of the Asian monsoon using stable isotopes. *SOLA* **1**, 113–116 (2005).
9. Craig, H. Isotopic variations in meteoric waters. *Science* **133**, 1702–1703 (1961).
10. Dansgaard, W. Stable isotopes in precipitation. *Tellus* **16**, 436–468 (1964).
11. Burnett, A. W., Mullins, H. T. & Patterson, W. P. Relationship between atmospheric circulation and winter precipitation $\delta^{18}\text{O}$ in central New York State. *Geophys. Res. Lett.* **31**, 4 (2004).
12. Koster, R. et al. Global sources of local precipitation as determined by the Nasa/Giss GCM. *Geophys. Res. Lett.* **13**, 121–124 (1986).
13. Jodar, J. et al. Vertical variation in the amplitude of the seasonal isotopic content of rainfall as a tool to jointly estimate the groundwater recharge zone and transit times in the Ordesa and Monte Perdido National Park aquifer system, north-eastern Spain. *Sci. Total Environ.* **573**, 505–517 (2016).
14. Bershaw, J. Controls on Deuterium Excess across Asia. *Geosciences* **8**, 257 (2018).
15. Kong, Y. L., Pang, Z. H. & Froehlich, K. Quantifying recycled moisture fraction in precipitation of an arid region using deuterium excess. *Tellus Ser. B-Chem. Phys. Meteorol.* **65**, 19251 (2013).
16. Schoenemann, S. W. & Steig, E. J. Seasonal and spatial variations of ^{17}O excess and complexity in Antarctic precipitation: Insights from an intermediate complexity isotope model. *J. Geophys. Res.* **121**, 11215–11247 (2016).
17. Wang, S. J., Zhang, M. J., Chen, Y. J., Zhu, X. F. & Liu, X. M. Influence of below-cloud evaporation on deuterium excess in precipitation of arid central Asia and its meteorological controls. *J. Hydrometeorol.* **17**, 1973–1984 (2016).
18. Jouzel, J. & Merlivat, L. Deuterium and oxygen 18 in precipitation: modeling of the isotope effects during snow formation. *J. Geophys. Res.-Atmos.* **89**, 11749–11757 (1984).
19. Jouzel, J., Froehlich, K. & Schotterer, U. Deuterium and oxygen-18 in present-day precipitation: data and modelling. *Hydrol. Sci. J.* **42**, 747–763 (1997).
20. Merlivat, L. & Jouzel, J. Global climatic interpretation of the deuterium-oxygen 18 relationship. *J. Geophys. Res.* **84**, 5029–5033 (1979).
21. Sha, L. J. et al. A novel application of triple oxygen isotope ratios of speleothems. *Geochim. Cosmochim. Acta.* **270**, 360–378 (2020).
22. Duan, P. Z. et al. Comparison of mass spectrometry and spectroscopy methods applied to measurements of water triple oxygen isotopic compositions. *Chi. Sci. Bull.* **66**, 4691–4699 (2021).
23. Steig, E. J. et al. Calibrated high-precision ^{17}O -excess measurements using laser-current tuned cavity ring-down spectroscopy. *Atmos. Meas. Tech.* **7**, 2421–2435 (2014).
24. Barkan, E. & Luz, B. High precision measurements of $^{17}\text{O}/^{16}\text{O}$ and $^{18}\text{O}/^{16}\text{O}$ ratios in H_2O . *Rapid Commun. Mass Sp.* **19**, 3737–3742 (2005).
25. Luz, B. & Barkan, E. Variations of $^{17}\text{O}/^{16}\text{O}$ and $^{18}\text{O}/^{16}\text{O}$ in meteoric waters. *Geochim. Cosmochim. Acta.* **74**, 6276–6286 (2010).
26. Barkan, E. & Luz, B. Diffusivity fractionations of $\text{H}_2^{16}\text{O}/\text{H}_2^{17}\text{O}$ and $\text{H}_2^{16}\text{O}/\text{H}_2^{18}\text{O}$ in air and their implications for isotope hydrology. *Rapid Commun. Mass Sp.* **21**, 2999–3005 (2007).
27. Risi, C. et al. Understanding the ^{17}O -excess glacial–interglacial variations in Vostok precipitation. *J. Geophys. Res. Atmos.* **115**, 1–15 (2010).
28. Risi, C., Landais, A., Winkler, R. & Vimeux, F. Can we determine what controls the spatio-temporal distribution of d-excess and ^{17}O -excess in precipitation using the LMDZ general circulation model? *Clim. Past* **9**, 2173–2193 (2013).
29. Li, S., Levin, N. E. & Chesson, L. A. Continental scale variation in ^{17}O -excess of meteoric waters in the United States. *Geochim. Cosmochim. Acta.* **164**, 110–126 (2015).
30. Uechi, Y. & Uemura, R. Dominant influence of the humidity in the moisture source region on the ^{17}O -excess in precipitation on a subtropical island. *Earth Planet. Sci. Lett.* **513**, 20–28 (2019).
31. Aron, P. G. et al. Triple oxygen isotopes in the water cycle. *Chem. Geol.* **565**, 120026 (2021).
32. Aggarwal, P. K., Longstaffe, F. J. & Schwartz, F. W. Ice Core ^{17}O reveals past changes in surface air temperatures and stratosphere to troposphere mass exchange. *Atmosphere* **14**, 1268 (2023).
33. Xia, Z. Y., Surma, J. & Winnick, M. J. The response and sensitivity of deuterium and ^{17}O excess parameters in precipitation to hydroclimate processes. *Earth-Sci. Rev.* **242**, 104432 (2023).
34. Wei, T. et al. A skilful prediction scheme for West China autumn precipitation. *Theor. Appl. Climatol.* **135**, 183–192 (2019).
35. Wei, T., He, S., Yan, Q., Dong, W. & Wen, X. Decadal Shift in West China Autumn Precipitation and its Association With Sea Surface Temperature. *J. Geophys. Res.-Atmos.* **123**, 835–847 (2018).
36. Yuan, X. & Liu, X. F. Onset-withdrawal dates of autumn persistent rains over western China and the associated autumn winter evolution of the atmospheric circulation. *Acta Meteorol. Sin.* **71**, 913–924 (2013).
37. Zhou, B. B. et al. Strengthening of the relationship between West China Autumn Rain and arctic oscillation in the mid-1980s. *Atmospheric Research* **265**, 105916 (2022).
38. Zhang, C. et al. Trends in autumn rain of West China from 1961 to 2014. *Theor. Appl. Climatol.* **135**, 533–544 (2019).
39. Chen, Y., Guo, M. & Qian, H. Effect of ENSO on the annual precipitation anomaly in Guanzhong Basin and southern Shaanxi China. *WRE 2019* **344**, 012090 (2019b).
40. Xie, C. et al. Precipitation stable isotope composition, moisture sources, and controlling factors in Xi'an, Northwest China. *Atmos. Res.* **280**, 106428 (2022).
41. Tang, Y. et al. Effects of changes in moisture source and the upstream rainout on stable isotopes in precipitation—a case study in Nanjing, eastern China. *Hydrol. Earth Syst. Sci.* **19**, 4293–4306 (2015).
42. Li, Y. Y. et al. Response characteristics of atmospheric boundary layer height to summer monsoon activity and monsoon precipitation of monsoon swing region in the eastern part of Northwest China. *Arid Land Geogr* **43**, 1169–1178 (2020).
43. Zhou, T. J. et al. Why the western Pacific subtropical high has extended westward since the late 1970s. *J. Climate* **8**, 22 (2009).
44. Draxler, R. R. & Hess, G. D. An overview of the HYSPLIT_4 modeling system for trajectories, dispersion, and deposition. *Aust. Meteorol. Mag.* **47**, 295–308 (1998).
45. Stein, A. et al. NOAA's HYSPLIT atmospheric transport and dispersion modeling system. *Bull. Am. Meteorol. Soc.* **96**, 2059–2077 (2015).
46. Xu, H. et al. Juxta position of western Pacific subtropical high on Asian Summer Monsoon shapes subtropical East Asian precipitation. *Geophys. Res. Lett.* **47**, e2019GL084705 (2020).
47. Ding, Y. & Chan, J. C. The East Asian summer monsoon: an overview. *Meteorol. Atmos. Phys.* **89**, 117–142 (2005).
48. Ding, Y. H. The Summer Monsoon in East Asia, in *Monsoons over China*. Springer Netherlands, Dordrecht (1994).
49. Zhou, T. J. & Yu, R. C. Atmospheric water vapor transport associated with typical anomalous summer rainfall patterns in China. *J. Geophys. Res.* **110**, D08104 (2005).

50. He, S. et al. Understanding tropical convection through triple oxygen isotopes of precipitation from the maritime continent. *J. Geophys. Res.* **126**, e2020JD033418 (2021).
51. Surma, J., Assonov, S. & Staubwasser, M. Triple oxygen isotope systematics in the hydrologic cycle. *Rev. Mineral. Geochem.* **86**, 401–428 (2021).
52. Gázquez, F., Calaforra, J. M., Evans, N. P. & Hodell, D. A. Using stable isotopes ($\delta^{17}\text{O}$, $\delta^{18}\text{O}$ and δD) of gypsum hydration water to ascertain the role of water condensation in the formation of subaerial gypsum speleothems. *Chem. Geol.* **452**, 34–46 (2017).
53. Li, Y. et al. Variations of stable isotopic composition in atmospheric water vapor and their controlling factors—a 6-year continuous sampling study in nanjing, eastern china. *J. Geophys. Res.* **125**, e2019JD031697 (2020).
54. Risi, C., Bony, S. & Vimeux, F. Influence of convective processes on the isotopic composition ($\delta^{18}\text{O}$ and δD) of precipitation and water vapor in the tropics: 2. Physical interpretation of the amount effect. *J. Geophys. Res.* **113**, D19306 (2008).
55. Bony, S., Risi, C. & Vimeux, F. Influence of convective processes on the isotopic composition ($\delta^{17}\text{O}$, δD) of precipitation and water vapor: 1. Radiative-convective equilibrium and Tropical Ocean-Global Atmosphere- Coupled Ocean-Atmosphere Response Experiment (TOGA-COARE) simulations. *J. Geophys. Res.* **113**, D1930 (2008).
56. Giménez, R., Bartolome, M., Gazquez, F., Iglesias, M. & Moreno, A. Underlying climate controls in triple oxygen (^{16}O , ^{17}O , ^{18}O) and hydrogen (^1H , ^2H) isotopes composition of rainfall (Central Pyrenees). *Front. Earth Sci-PRC.* **9**, 1–16 (2021).
57. Landais, A. et al. Combined measurements of ^{17}O excess and d-excess in African monsoon precipitation: Implications for evaluating convective parameterizations. *Earth Planet. Sci. Lett.* **298**, 104–112 (2010).
58. Aron, P. G., Li, S., Brooks, J. R., Welker, J. M. & Levin, N. E. Seasonal variations in triple oxygen isotope ratios of precipitation in the Western and Central United States. *Paleoceanogr. Paleoclimatol.* **38**, e2022PA004458 (2023).
59. Surma, J., Assonov, S., Bolourchi, M. J. & Staubwasser, M. Triple oxygen isotope signatures in evaporated water bodies from the Sistan Oasis, Iran. *Geophys. Res. Lett.* **42**, 8456–8462 (2015).
60. Aggarwal, P. K. et al. Proportions of convective and stratiform precipitation revealed in water isotope ratios. *Nat. Geosci.* **9**, 624–629 (2016).
61. Konecky, B. L., Noone, D. C. & Cobb, K. M. The influence of competing hydroclimate processes on stable isotope ratios in tropical rainfall. *Geophys. Res. Lett.* **46**, 1622–1633 (2019).
62. Stewart, M. K. Stable isotope fractionation due to evaporation and isotopic exchange of falling water drops: applications to atmospheric processes and evaporation of lakes. *J. Geophys. Res.* **80**, 1133–1146 (1975).
63. Lee, J.-E., Fung, I., DePaolo, D. J. & Otto-Bliesner, B. Water isotopes during the Last Glacial Maximum: New general circulation model calculations. *J. Geophys. Res.* **113**, D19109 (2008).
64. Graf, P., Wernli, H., Pfahl, S. & Sodemann, H. A new interpretative framework for below-cloud effects on stable water isotopes in vapour and rain. *Atmos. Chem. Phys.* **19**, 747–765 (2019).
65. Tian, C. et al. Spatial and temporal variations of tap water ^{17}O -excess in China. *Geochim. Cosmochim. Acta.* **260**, 1–14 (2019).
66. Matejka, T. J., Houze, R. A. Jr. & Hobbs, P. V. Microphysics and dynamics of clouds associated with mesoscale rainbands in extratropical cyclones. *Q. J. R. Meteorol. Soc.* **106**, 29–56 (1980).
67. Jeelani, G. et al. Hydrological processes in glacierized high-altitude basins of the western Himalayas. *Hydrogeol. J.* **26**, 615–628 (2018).
68. Landais, A. et al. Triple isotopic composition of oxygen in surface snow and water vapor at NEEM (Greenland). *Geochim. Cosmochim. Acta.* **77**, 304–316 (2012).
69. Tian, L. D. et al. Stable isotopic variations in west China: A consideration of moisture sources. *J. Geophys. Res.* **112**, D10112 (2007).
70. Passey, B. H. & Levin, N. E. Triple oxygen isotopes in meteoric waters, carbonates, and biological apatites: Implications for continental paleoclimate reconstruction. *Rev. Mineral. Geochem.* **86**, 429–462 (2021).
71. Schoenemann, S. W., Schauer, A. J. & Steig, E. J. Measurement of SLAP2 and GISP $\delta^{17}\text{O}$ and proposed VSMOW-SLAP normalization for $\delta^{17}\text{O}$ and ^{17}O -excess. *Rapid Commun. Mass Sp.* **27**, 582–590 (2013).
72. Kanamitsu, M. et al. NCEP–DOE AMIP-II reanalysis (R-2). *B. Am. Meteorol. Soc.* **83**, 1631–1644 (2002).
73. Hersbach, H., et al. ERA5 hourly data on single levels from 1940 to present. *Copernicus Climate Change Service (C3S) Climate Data Store (CDS)* (2023).
74. Song, Y. & Wei, J. Diurnal cycle of summer precipitation over the North China Plain and associated land–atmosphere interactions: Evaluation of ERA5 and MERRA-2. *Int. J. Climatol.* **41**, 6031–6046 (2021).
75. Kalnay, E. et al. The NCEP/NCAR 40-year reanalysis project. *Bull. Am. Meteorol. Soc.* **77**, 437–471 (1996).
76. Sodemann, H., Schwierz, C. & Wernli, H. Interannual variability of Greenland winter precipitation sources: Lagrangian moisture diagnostic and North Atlantic Oscillation influence. *Geophys. Res. Lett.* **113**, D03107–D03123 (2008).
77. Krklec, K., Domínguez-Villar, D. & Lojen, S. The impact of moisture sources on the oxygen isotope composition of precipitation at a continental site in central Europe. *J. Hydrol.* **561**, 810–821 (2018).

Acknowledgements

This work was supported by grants from the National Natural Science Foundation of China (Nos. 42103005, 41888101, 42003006, and 42106228). Y.F. Ning is greatly appreciated for his mentoring in all laboratory aspects. We are also grateful for the comments from three anonymous reviewers and editors Dr. Yama Dixit and Dr. Clare Davis that helped us significantly improve the manuscript.

Author contributions

H.C. and L.J.S. designed the project. L.J.S. and B.Y.Z. collected the precipitation samples. L.J.S. performed the triple oxygen isotope analysis. L.F.S. made the map. Q.S.L. computed the back-trajectories. Y.X.L., X.J.W. and H.P. run the model for convective precipitation, stratiform precipitation, and total precipitation. X.J.W. analyzed the pattern of the Western Pacific Subtropical High on a daily scale. L.J.S. wrote the manuscript with input from L.J.T. and P.Z.D. All authors contributed to revising the manuscript at various stages.

Competing interests

The authors declare no competing interests.

Additional information

Supplementary information The online version contains supplementary material available at <https://doi.org/10.1038/s43247-024-01354-2>.

Correspondence and requests for materials should be addressed to Pengzhen Duan or Hai Cheng.

Peer review information *Communications Earth & Environment* thanks the anonymous reviewers for their contribution to the peer review of this work. Primary Handling Editors: Yama Dixit, Clare Davis and Martina Grecequet. A peer review file is available.

Reprints and permissions information is available at <http://www.nature.com/reprints>

Publisher's note Springer Nature remains neutral with regard to jurisdictional claims in published maps and institutional affiliations.

Open Access This article is licensed under a Creative Commons Attribution 4.0 International License, which permits use, sharing, adaptation, distribution and reproduction in any medium or format, as long as you give appropriate credit to the original author(s) and the source, provide a link to the Creative Commons licence, and indicate if changes were made. The images or other third party material in this article are included in the article's Creative Commons licence, unless indicated otherwise in a credit line to the material. If material is not included in the article's Creative Commons licence and your intended use is not permitted by statutory regulation or exceeds the permitted use, you will need to obtain permission directly from the copyright holder. To view a copy of this licence, visit <http://creativecommons.org/licenses/by/4.0/>.

© The Author(s) 2024